NANO LETTERS

LETTER

pubs.acs.org/NanoLett

Nanoimprint Lithography for High-Efficiency Thin-Film Silicon Solar Cells

Corsin Battaglia,* Jordi Escarré, Karin Söderström, Lukas Erni, Laura Ding, Grégory Bugnon, Adrian Billet, Mathieu Boccard, Loris Barraud, Stefaan De Wolf, Franz-Josef Haug, Matthieu Despeisse, and Christophe Ballif

Ecole Polytechnique Fédérale de Lausanne (EPFL), Institute of Microengineering (IMT), Photovoltaics and Thin Film Electronics Laboratory, 2000 Neuchâtel, Switzerland

Supporting Information

ABSTRACT: We demonstrate high-efficiency thin-film silicon solar cells with transparent nanotextured front electrodes fabricated via ultraviolet nanoimprint lithography on glass substrates. By replicating the morphology of state-of-the-art nanotextured zinc oxide front electrodes known for their exceptional light trapping properties, conversion efficiencies of up to 12.0% are achieved for micromorph tandem junction cells. Excellent light incoupling results in a remarkable summed short-circuit current density of 25.9 mA/cm^2 for amorphous top cell and microcrystalline bottom cell thicknesses of only 250 and 1100 nm, respectively. As efforts to maximize light harvesting continue, our study validates nanoimprinting as a versatile tool to investigate nanophotonic effects of a large variety of nanostructures directly on device performance.

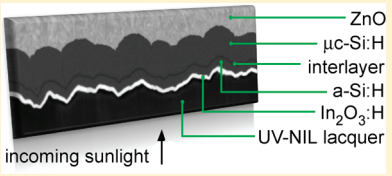

KEYWORDS: photovoltaics, thin-film silicon solar cells, micromorph tandem junction, nanoimprinting, light trapping

Advanced light trapping concepts are crucial to realize high-efficiency thin-film silicon solar cells, as the absorption coefficient of silicon is small in the near-infrared region. With properly engineered photonic nanostructures, sunlight can be trapped within the thin absorbing silicon layers, thereby enhancing light absorption and thus conversion efficiencies. Recently, exciting new strategies for improving light harvesting have gained tremendous interest, including nanopillar- and nanohole-type geometries,[1−6] plasmonics and guided modes,[7−12] and photonic crystals.[13−15]

Light scattering at nanotextured interfaces provides a powerful and proven alternative to improve the optical performance of thin-film silicon devices.[16−27] However, despite intensive experimental and theoretical efforts, neither the ideal interface morphology nor the ideal scattering characteristics have been identified to date. From an experimental point of view, one desires a method that allows one to evaluate and compare the light-trapping capabilities of specifically designed photonic nanostructures directly in the device. Ultraviolet nanoimprint lithography (UV-NIL) provides exactly such a platform. Feature sizes much smaller than those relevant to visible and near-infrared light scattering have been reproduced using UV-NIL,[28] allowing full flexibility for fabricating and integrating a large variety of surface morphologies into functional solar cells.[29] Among the many unconventional nanopatterning techniques that have been developed during recent years, UV-NIL further stands out as a promising technology for high-throughput large-area nanoscale patterning at low cost, as is required for photovoltaic applications.[30]

Although a huge potential for boosting the performance of thin-film solar cells has been attributed to UV-NIL for some time, a clear demonstration of its capabilities in terms of conversion efficiency is so far lacking. Previously, in a proof-of-concept study, we reported efficiencies of 7.2% for single junction microcrystalline silicon (μc-Si:H) solar cells deposited on nanotextured electrodes fabricated via UV-NIL.[29] Although we achieved respectable current densities, cell efficiencies were limited by massive ohmic losses in the front contact caused by the high current density and low voltage produced by the μc-Si:H cell. Here, we solved this problem by integrating transparent front electrodes fabricated by UV-NIL into a micromorph tandem junction solar cell, consisting of a high-gap amorphous silicon (a-Si:H) and a low-gap μc-Si:H solar cell stack on a glass substrate. The much more favorable voltage-to-current ratio of the tandem configuration combined with excellent light trapping provided by the nanoimprinted front electrode allows us to reach initial conversion efficiencies of 12.0%. This value proves that nanoimprinting allows one to go far beyond proof-of-concept devices, as it is as high as for cells on state-of-the-art nanotextured zinc oxide (ZnO) electrodes.

For the case study presented here, we use the randomly oriented pyramidal self-texture of state-of-the-art ZnO, known for its exceptional light trapping properties,[16−18] as a master for the UV-NIL replication process. This allows direct comparison of the performance of the cell grown on the UV-NIL replica and the ZnO master, which serves as a benchmark. Boron-doped ZnO

Received: October 27, 2010
Revised: December 17, 2010

   dx.doi.org/10.1021/nl1037787 | *Nano Lett.* XXXX, XXX, 000–000

layers with electron mobility μ = 37 cm^2/V·s, carrier density n = 4 × 10^{19} cm^{-3}, resistivity ρ = 4 × 10^{-3} Ω·cm, thickness t = 4.8 μm, and sheet resistance R_{sh} = 8 Ω/□ were grown via low-pressure chemical vapor deposition (LP-CVD)[31] on 0.5 mm thick borosilicate glass without antireflection coating. To optimize the morphology for the growth of the cells, the ZnO surface was treated for 20 min with an argon plasma.[32]

A negative UV-NIL stamp was fabricated by nanoimprinting of the master ZnO texture into a UV sensitive sol−gel lacquer (Ormocer from Micro Resist Technology GmbH). After curing under UV light and demolding, this stamp was coated with an antisticking layer and used to transfer the positive structure onto a UV-NIL lacquer on a borosilicate glass substrate. More details on our high-fidelity UV-NIL process may be found in refs 33 and 34.

Subsequently, a high-mobility hydrogenated indium oxide (In_2O_3:H) layer[35] with carrier mobility μ = 104 cm^2/V·s, carrier density n = 1.1 × 10^{20} cm^{-3}, resistivity ρ = 5 × 10^{-4} Ω·cm, thickness t = 110 nm, and sheet resistance R_{sh} = 45 Ω/□ was sputtered onto the replicated structures and covered by a thin sputtered aluminum-doped ZnO layer of thickness t = 20 nm that serves as a protective barrier layer against the hydrogen-rich plasma during the subsequent silicon deposition.

Micromorph silicon solar cells of size 5 × 5 mm^2 were deposited by plasma-enhanced chemical vapor deposition in an industrial KAI reactor. The micromorph concept, pioneered in our lab 15 years ago,[36,37] has been identified as one of the most promising thin-film technologies for lowering the cost of photovoltaic energy, as it is based on abundant, nontoxic materials and low-temperature processes.[38] The micromorph tandem cells consist of an a-Si:H top cell with intrinsic layer thickness of 250 nm and a μc-Si:H bottom cell with intrinsic layer thickness of 1.1 μm. A resistive SiO_x interlayer was incorporated between the amorphous and microcrystalline subcells as described in ref 39 to limit undesired local current drains caused by the roughness of the substrate. This layer simultaneously serves as an intermediate reflector that boosts the absorption in the amorphous top cell.[40] A white, quasi-Lambertian dielectric back reflector was mounted behind the back electrode for characterization.

External quantum efficiencies EQEs of the a-Si:H top and μc-Si:H bottom cells (EQE_{top} and EQE_{bot}) were measured under red and blue bias light illumination, respectively. The corresponding short-circuit current densities J_{sc}^{top} and J_{sc}^{bot} were calculated from the EQE curves by convolution with the photon flux of the global air mass 1.5 ($AM1.5_g$) solar spectrum. The summed short-circuit current density $J_{sc}^{sum} = J_{sc}^{top} + J_{sc}^{bot}$ does not represent a real current flowing through the device but is a useful quantity to characterize the absorption, that is, the light trapping, in the cell, as it allows direct comparison with single junction cell current densities. The current density−voltage $J(V)$ characteristics, from which the open-circuit voltages V_{oc} and the fill factors FF were determined, were measured using a dual lamp sun simulator in standard test conditions (25 °C, $AM1.5_g$, 1000 W/m^2). They were normalized by the J_{sc} value of the current-limiting subcell from the EQE measurement.

Figure 1a presents a scanning electron microscopy (SEM) image of a cross section milled with a focused ion beam (FIB) through the micromorph cell deposited on the replicated substrate. Inspection of Figure 1a reveals the dark nanotextured UV-NIL lacquer, followed by the conformal In_2O_3:H layer, which appears bright. Comparison of atomic force microscopy (AFM) images of the master ZnO substrate and its corresponding UV-NIL replica shown in Figure 2 indicates the high quality of the replication process (for a quantitative fidelity analysis of the replication process and a detailed comparison between optical properties of master and replica, see refs 29 and 33).

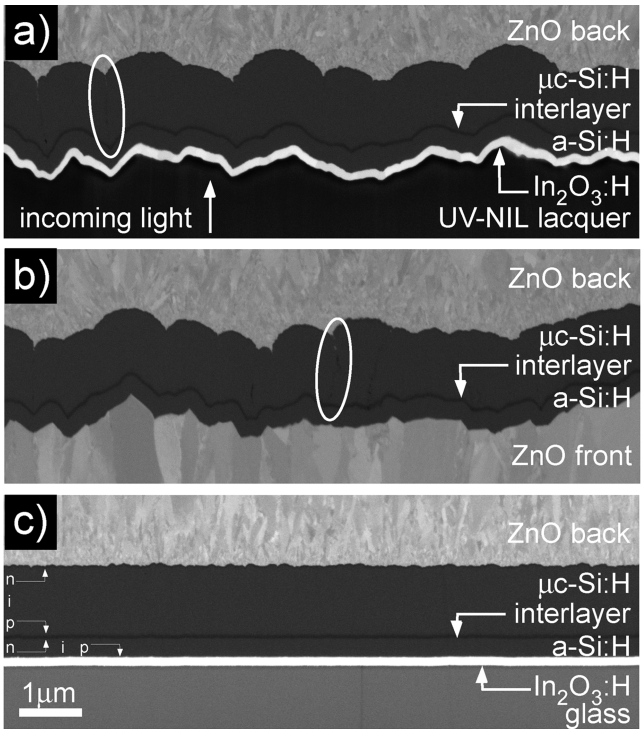

Figure 1. FIB cuts across the three solar cell structures imaged by SEM: (a) UV-NIL replica with In_2O_3:H, (b) master ZnO superstrate, (c) flat glass superstrate with In_2O_3:H. White ellipses indicate the position of texture-induced cracks in the microcrystalline layer. In (c) we also show the location of the thin p- and n-type doped silicon layers, which however do not exhibit sufficient contrast to be distinguished from the intrinsic (i) silicon layers.

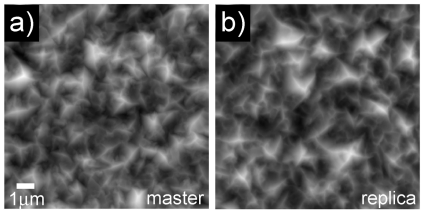

Figure 2. AFM topographies of the pyramidal self-texture: (a) ZnO master, (b) corresponding UV-NIL replica.

On top of the front electrode, the amorphous top cell is clearly separated from the microcrystalline bottom cell by the resistive interlayer, which appears darker compared to the intrinsic silicon layers. Although μc-Si:H does not give significant grain contrast, some boundaries between dense grain conglomerates (known as cracks and marked by white ellipses in Figure 1) may be observed. The cracks, caused by the growth dynamics of the microcrystalline grains on the rough substrate, have been shown to be detrimental to V_{oc} and FF, as they act as local current drains.[41] The ideal surface texture must therefore not only maximize the light trapping in the cell, but must also minimize cracks in the absorbing layer.

To allow for a quantitative assessment of the light trapping capabilities of the replicated substrate with respect to a nontextured substrate, we also deposited a full micromorph cell without light trapping on a flat glass substrate coated with In_2O_3:H, shown in

dx.doi.org/10.1021/nl1037787 |Nano Lett. XXXX, XXX, 000–000

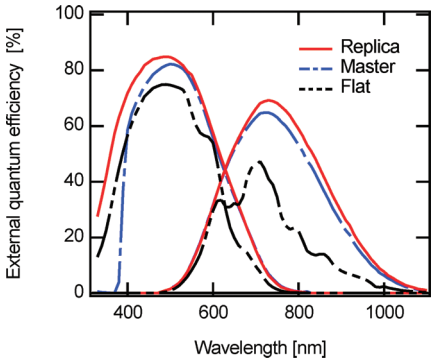

Figure 3. EQE of micromorph solar cells fabricated on the replicated nanotextured substrate and its master. The measurement for the flat substrate is also shown.

Figure 1c. However, a more pragmatic benchmark for cell performance is provided by the cell grown directly on the master LP-CVD ZnO (Figure 1b).

Figure 3 presents EQE measurements for the three cells. The amorphous top cell absorbs the blue and green part of the spectrum between 350 and 800 nm, while the microcrystalline bottom cell absorbs the red and infrared part of the spectrum from 500 to 1100 nm. We first discuss the spectral responses of the microcrystalline subcells, which benefit most from good light trapping, because of the low absorption coefficient at long wavelengths. As can be seen from Figure 3, the EQE measurement for the microcrystalline cell on the flat substrate exhibits interference fringes as incoming light and light reflected at the intermediate and back reflectors superimposes constructively and destructively. The effect of light trapping is dramatically demonstrated by the almost 2-fold enhancement of the photogenerated current when nanotextured interfaces are introduced (see Table 1). Comparing the spectral responses of the microcrystalline bottom cells deposited on the replica and its master, it can also be seen that the replica exhibits an improved infrared response compared to its master, accounting for a gain in J_{sc}^{bot} of 0.9 mA/cm^2. This can be understood by considering the absorption caused by free carriers in the front electrode (see Supporting Information). Although the carrier density of In_2O_3:H is higher by a factor of 2−3 compared to ZnO, its high carrier mobility and reduced thickness (40 times thinner than the ZnO layer) significantly reduce free carrier absorption responsible for parasitic absorption in the near-infrared.[42]

Focusing now on the EQEs of the amorphous top cells, we see that the current enhancement in the top cell upon introduction of nanotextured interfaces is not as high as for the bottom cell, as most of the blue and green light is absorbed during the first pass through the amorphous cell. However, the nanotextured interface between the front electrode and the silicon serves to reduce reflection of light out of the cell as the effective refractive index changes gradually across the rough interface. Note also that, because all cells were deposited in the same run to allow direct comparison, the thickness of the doped layers is not optimized for the flat cell geometry and some additional parasitic absorption occurs due to their higher thickness. Furthermore we observe an improved blue response of the replica compared to the master, accounting for a substantial gain in J_{sc}^{top} of 1.0 mA/cm^2. This gain is due to the larger band gap of In_2O_3:H (330 nm) with respect to ZnO (380 nm) (see Supporting Information). In addition, for the master structure a small amount of light is specularly reflected at the flat glass-ZnO interface (2% at normal incidence), whereas the textured lacquer-In_2O_3:H interface (having approximately the same refractive index contrast as the glass-ZnO interface) acts again as a graded index antireflection layer.

Table 1. Characteristics of Micromorph Solar Cells Fabricated on Textured Replica, Corresponding Master, and Flat Superstrate

substrate	J_{sc}^{top} [mA/cm^2]	J_{sc}^{bot} [mA/cm^2]	V_{oc} [mV]	FF [%]	efficiency [%]
replica	12.9	13.0	1359	68.7	12.0
master	11.9	12.1	1385	72.6	12.0
flat	10.4	6.7	1421	81.2	7.7

As the micromorph tandem structure is a two-terminal device, where top and bottom cell are connected in series, the current generated by each component cell should be equal (a slight mismatch may be beneficial to improve fill factor and consequently efficiency[43]). In principle, current matching between the two subcells is achieved by tuning the thickness of the respective intrinsic absorber layers. However, in practice, the thickness of the amorphous top cell must be kept to a minimum in order to mitigate the effects of light induced degradation due to the Staebler−Wronski effect.[44] At the same time, on an industrial and ultimately on an economic level it is of interest to keep the microcrystalline bottom cell as thin as possible also[45] and compensate the current losses with an efficient light trapping scheme. Inspection of Table 1 reveals that both cells deposited on the nanotextured substrates are almost perfectly matched. Because of the simultaneous current gain in the top and the bottom cell on the replicated superstrate, matched and summed currents of 12.9 and 25.9 mA/cm^2 are achieved, a remarkable results for such a thin (only 1.1 μm) microcrystalline layer (see, for example, ref 20 for comparison, in which matched and summed currents of 12.7 and 26.0 mA/cm^2 are obtained for a 3 μm thick microcrystalline absorber layer).

We now turn to the $J(V)$ characteristics shown in Figure 4. Performance metrics of the cells are summarized in Table 1. As mentioned in the introduction, the micromorph tandem configuration has the advantage of a higher impedance compared to a single junction solar cell. As proposed by Hanak,[46] the reduction in fill factor FF due to resistive losses in the front electrode can be estimated using the ratio of the Ohmic power loss $R_{sh}J_{MPP}^2$ and the maximum achievable power $J_{MPP}V_{MPP}$

$$FF = 100\% - \left(\frac{R_{sh}J_{MPP}}{V_{MPP}}\right)\left(\frac{w^2}{3}\right) - \Delta FF$$

Here R_{sh} is the sheet resistance of the front electrode and MPP represents the maximum power point of the $J(V)$ curve. The factor $w^2/3$ takes into account the measurement and cell geometry with w as the cell width. ΔFF represents all other losses such as resistive losses in the silicon layers and the back electrode, as well as contact resistances and the resistance of the recombination junction between the amorphous and microcrystalline subcells.

Filling in typical values for a microcrystalline cell (V_{MPP} = 400 mV, J_{MPP} = 22 mA/cm^2) and a micromorph cell (V_{MPP} = 1100 mV, J_{MPP} = 11 mA/cm^2) and using the sheet resistance of the In_2O_3:H layer (R_{sh} = 45 Ω/□), we find that the FF should increase substantially by an estimated absolute 17% when going from the microcrystalline to the micromorph cell configuration, rendering

dx.doi.org/10.1021/nl1037787 |Nano Lett. XXXX, XXX, 000–000

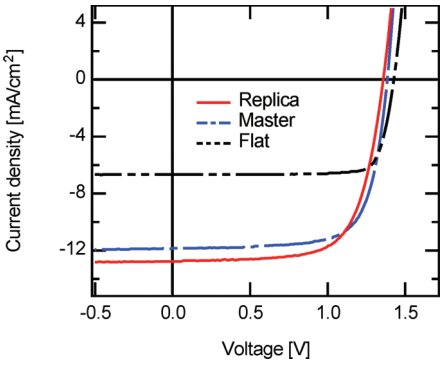

Figure 4. $J(V)$ characteristics of micromorph solar cells fabricated on the replicated nanotextured substrate and its master. The measurement for the flat substrate is also shown.

the micromorph tandem cell much more tolerant of series resistance losses in the front electrode. For the cells on ZnO ($R_{sh} = 8\ \Omega/\square$) the effect is not as pronounced, as the change from single junction to tandem junction improves the FF by only 3%. Although crudely estimated, these values correctly reproduce the trend in experiment, where we observe an increase of the FF by almost 12% for the replica with In_2O_3:H, but only 2% for the ZnO master when going from the microcrystalline (not shown) to the micromorph configuration.

The absolute 12% increase in fill factor leads to a dramatic improvement of the cell efficiency. Compared to our earlier report on microcrystalline cells, we were able to improve the efficiency by almost 5% (absolute), achieving an initial efficiency of 12.0% for the micromorph cell on the replica, that is, the same efficiency as for the micromorph cell on the state-of-the-art ZnO master. It should be noted that the slightly lower V_{oc} and FF of the cell on the replica is compensated by the overall higher transparency of the In_2O_3:H front electrode, resulting in a higher J_{sc}. The lower *FF* can be explained partially by the higher sheet resistance of the In_2O_3:H layer with respect to the ZnO. However, it is also possible that the combined reduction of FF and V_{oc} points toward a slightly higher crack density in μc-Si:H on the replicated substrate.[41] This could explain the discrepancy between the estimated 17% and the observed 12% improvement in *FF* when going from single to tandem junction. A detailed statistical analysis of the crack distribution[47] is out of the scope of the present work. However, new approaches to reduce the number of cracks and to limit their negative impact on the V_{oc} and FF of the cells are currently being intensively investigated in our lab. Promising first results[18] provide a clear roadmap for maximizing light trapping without paying the price of reduced electrical cell performance.

Our case study in which we replicated the morphology of ZnO validates UV-NIL as a platform to test and evaluate the light trapping potential of a wide range of nanostructures directly in functional high-efficiency solar cells. For the superstrate configuration, this opens the door to exciting new possibilities as one is no longer bound to the self-texture mechanisms of ZnO and tin oxide (SnO_2). Not only transparent structures may serve as a master for the replication process but also structures fabricated from opaque materials, such as thermally roughened silver films,[48] that are often used at the back electrode in the substrate configuration. More exotic nanostructures such as self-ordered dimple patterns obtained via anodic oxidation of aluminum[12] or nanopillar-type structures fabricated via nanosphere lithography,[1,2] both of which have shown impressive results in the substrate configuration, may be transferred to transparent superstrates.

In conclusion, we demonstrated for the first time a thin-film silicon solar cell on a replicated substrate fabricated by UV-NIL with an efficiency well above 10% using the micromorph tandem configuration. The achieved initial efficiency of 12.0% is as high as for the cell fabricated on a state-of-the-art ZnO substrate, which serves as a benchmark. Furthermore, a substantial 1.9 mA/cm^2 improvement in the summed short-circuit current density was demonstrated, resulting in a summed short-circuit current of 25.9 mA/cm^2 for a microcrystalline bottom cell thickness of only 1.1 μm. Our approach holds the promise for significant further efficiency improvements, not only by careful device optimization and loss reduction, but by providing a general and versatile tool for engineering and investigating transparent nanophotonic structures for integration into high-efficiency solar cells and modules.

■ ASSOCIATED CONTENT

Supporting Information. Additional figure of absorptance measurements for In_2O_3:H electrode and ZnO electrode. This material is available free of charge via the Internet at http://pubs.acs.org.

■ AUTHOR INFORMATION

Corresponding Author
*E-mail: corsin.battaglia@epfl.ch.

■ ACKNOWLEDGMENT

We acknowledge Peter Cuony and Takashi Koida for fruitful discussions, Duncan Alexander for assistance with the FIB, Zachary Holman for careful proofreading of the manuscript, and the Swiss Federal Energy Office and the Swiss National Science Foundation for funding under Project No. 101191 and Grant 200021 12577/1.

■ REFERENCES

(1) Zhu, J.; Hsu, C.-M.; Yu, Z.; Fan, S.; Cui, Y. *Nano Lett.* **2010,** *10,* 1979.
(2) Naughton, M. J.; et al. *Phys. Status Solidi RRL* **2010,** *4,* 181.
(3) Garnett, E.; Yang, P. *Nano Lett.* **2010,** *10,* 1082.
(4) Kelzenberg, M. D.; Boettcher, S. W.; Petykiewicz, J. A.; Turner-Evans, D. B.; Putnam, M. C.; Warren, E. L.; Spurgeon, J. M.; Briggs, R. M.; Lewis, N. S.; Atwater, H. A. *Nat. Mater.* **2010,** *9,* 239.
(5) Cao, L.; Fan, P.; Vasudev, A. P.; White, J. S.; Yu, Z.; Cai, W.; Schuller, J. A.; Fan, S.; Brongersma, M. L. *Nano Lett.* **2010,** *10,* 439.
(6) Han, S. E.; Chen, G. *Nano Lett.* **2010,** *10,* 1012.
(7) Atwater, H. A.; Polman, A. *Nat. Mater.* **2010,** *9,* 205.
(8) Söderström, K.; Haug, F.-J.; Escarré, J.; Cubero, O.; Ballif, C. *Appl. Phys. Lett.* **2010,** *96,* No. 213508.
(9) Ferry, V. E.; Verschuuren, M. A.; Li, H. B. T.; Verhagen, W.; Walters, R. J.; Schropp, R. E. I.; Atwater, H. A.; Polman, A. *Opt. Exp.* **2010,** *18,* A237.
(10) Eminian, C.; Haug, F.-J.; Cubero, O.; Niquille, X.; Ballif, C. *Prog. Photovolt: Res. Appl.* **2010** [Online early access]. DOI: 10.1002/pip.1015.
(11) Catchpole, K. R.; Polman, A. *Appl. Phys. Lett.* **2008,** *93,* No. 191113.
(12) Sai, H.; Fujiwara, H.; Kondo, M.; Kanamori, Y. *Appl. Phys. Lett.* **2008,** *93,* No. 143501.
(13) Bermel, P.; Luo, C.; Zeng, L.; Kimerling, L. C.; Joannopoulos, J. D. *Opt. Express* **2007,** *15,* 16986.
(14) Krc, J.; Zeman, M.; Luxembourg, S. L.; Topic, M. *Appl. Phys. Lett.* **2009,** *94,* No. 153501.
(15) Bielawny, A.; Rockstuhl, C.; Lederer, F.; Wehrspohn, R. B. *Opt. Express* **2009,** *17,* 8439.

(16) Benagli, S.; Borrello, D.; Vallat-Sauvain, E.; Meier, J.; Kroll, U.; Hoetzel, H.; Bailat, J.; Steinhauser, J.; Marmelo, M.; Monteduro, G.; Castens, L. Proceedings of the 24th European Photovoltaic Solar Energy Conference, Hamburg, Germany, 2009, 3BO.9.3.
(17) Bailat, J. et al. Proceedings of the 5th World Conference on Photovoltaic Energy Conversion, Valencia, Spain, 2010; p 2720.
(18) Despeisse, M.; Boccard, M.; Bugnon, G.; Cuony, P.; Söderström, T.; Parascandolo, G.; Stückelberger, M.; Charrière, M.; Löfgren, L.; Battaglia, C.; Hänni, S.; Billet, A.; Meillaud, F.; Ballif, C. Proceedings of the 5th World Conference on Photovoltaic Energy Conversion, Valencia, Spain, 2010; p 2793.
(19) Berginski, M.; Hüpkes, J.; Reetz, W.; Rech, B.; Wuttig, M. *Thin Solid Films* **2008,** *516*, 5836–5841.
(20) Dominé, D.; Buehlmann, P.; Bailat, J.; Billet, A.; Feltrin, A.; Ballif, C. *Phys. Status Solidi RRL* **2008,** *2*, 163–165.
(21) Hongsingthong, A.; Krajangsang, T.; Yunaz, I. A.; Miyajima, S.; Konagai, M. *Appl. Phys. Exp.* **2010,** *3*, No. 051103.
(22) Zhang, W.; Bunte, E.; Worbs, J.; Siekmann, H.; Kirchhoff, J.; Gordijn, A.; Hüpkes, J. *Phys. Status Solidi C* **2010,** *7*, 1120.
(23) Owen, J. I.; Hüpkes, J.; Zhu, H.; Bunte, E.; Pust, S. E. *Phys. Status Solidi A* **2010** [Online early access]. DOI: 10.1002/pssa.201026164.
(24) Boccard, M.; Cuony, P.; Battaglia, C.; Despeisse, M.; Ballif, C. *Phys. Status Solidi RRL* **2010** [Online early access]. DOI: 10.1002/pssr.201004303.
(25) Dominé, D.; Haug, F.-J.; Battaglia, C.; Ballif, C. *J. Appl. Phys.* **2010,** *107*, No. 044504.
(26) Jäger, K.; Zeman, M. *Appl. Phys. Lett.* **2009,** *95*, No. 171108.
(27) Rockstuhl, C.; Fahr, S.; Bittkau, K.; Beckers, T.; Carius, R.; Haug, F.-J.; Söderström, T.; Ballif, C.; Lederer, F. *Opt. Express* **2010,** *18*, A335.
(28) Guo, L. J. *Adv. Mater.* **2007,** *19*, 495.
(29) Battaglia, C.; Söderström, K.; Escarré, J.; Haug, F.-J.; Dominé, D.; Cuony, P.; Boccard, M.; Bugnon, G.; Denizot, C.; Despeisse, M.; Feltrin, A.; Ballif, C. *Appl. Phys. Lett.* **2010,** *96*, No. 213504.
(30) Ahn, S. H.; Guo, L. J. *ACS Nano* **2009,** *3*, 2304.
(31) Faÿ, S.; Steinhauser, J.; Oliveira, N.; Vallat-Sauvain, E.; Ballif, C. *Thin Solid Films* **2007,** *515*, 8558–8561.
(32) Bailat, J.; Dominé, D.; Schlüchter, R.; Steinhauser, J.; Faÿ, S.; Freitas, F.; Bucher, C.; Feitknecht, L.; Niquille, X.; Tscharner, T.; Shah, A.; Ballif, C. Proceedings of the 4th World Conference on Photovoltaic Energy Conversion, Waikoloa, Hawaii, 2006; p 1553.
(33) Escarré, J.; Söderström, K.; Haug, F.-J.; Battaglia, C.; Ballif, C. *Sol. Energy Mater. Sol. Cells* **2010** [Online early access]. DOI: 10.1016/j.solmat.2010.11.010.
(34) Söderström, K.; Escarré, J.; Cubero, O.; Haug, F.-J.; Perregaux, S.; Ballif, C. *Prog. Photovolt: Res. Appl.* **2010** [Online early access]. DOI: 10.1002/pip.1003.
(35) Koida, T.; Fujiwara, H.; Kondo, M. *Jpn. J. Appl. Phys.* **2007,** *46*, L685–L687.
(36) Shah, A.; Torres, P.; Tscharner, R.; Wyrsch, N.; Keppner, H. *Science* **1999,** *285*, 692.
(37) Shah, A. *Thin-film silicon solar cells*; EPFL Press, CRC Press: Boca Raton, FL, 2010.
(38) Aberle, A. G. *Thin Solid Films* **2009,** *517*, 4706.
(39) Despeisse, M.; Bugnon, G.; Feltrin, A.; Stueckelberger, M.; Cuony, P.; Meillaud, F.; Billet, A.; Ballif, C. *Appl. Phys. Lett.* **2010,** *96*, No. 073507.
(40) Buehlmann, P.; Bailat, J.; Dominé, D.; Billet, A.; Meillaud, F.; Feltrin, A.; Ballif, C. *Appl. Phys. Lett.* **2007,** *91*, 143505.
(41) Python, M.; Madani, O.; Dominé, D.; Meillaud, F.; Vallat-Sauvain, E.; Ballif, C. *Sol. Energy Mater. Sol. Cells* **2009,** *93*, 1714–1720.
(42) Coutts, T. J.; Young, D. L.; Li, X. *MRS Bull.* **2000,** *25*, 58.
(43) Dominé, D. Ph.D. Thesis, Université de Neuchâtel, Switzerland, 2009; p 107.
(44) Staebler, D. L.; Wronski, C. R. *Appl. Phys. Lett.* **1977,** *31*, 292.
(45) Parascandolo, G.; Barlome, R.; Bugnon, G.; Söderström, T.; Strahm, B.; Feltrin, A.; Ballif, C. *Appl. Phys. Lett.* **2010,** *96*, No. 233508.
(46) Hanak, J. J. *Solar Energy* **1979,** *23*, 145.
(47) Python, M.; Vallat-Sauvain, E.; Bailat, J.; Dominé, D.; Fesquet, L.; Shah, A.; Ballif, C. *J. Non-Cryst. Solids* **2008,** *354*, 2258.
(48) Banerjee, A.; Guha, S. *J. Appl. Phys.* **1991,** *69*, 1030.